Title

OpenFOAM predictions of hydrodynamics loads on full-scale TLP

Authors

Dai, Shaoshi
Younis, Bassam A
Sun, Liping

Publication Date

2015-07-01

DOI

10.1016/j.oceaneng.2015.04.042

Peer reviewed

Ocean Engineering 102 (2015) 162–173

Contents lists available at ScienceDirect

Ocean Engineering

journal homepage: www.elsevier.com/locate/oceaneng

OpenFOAM predictions of hydrodynamics loads on full-scale TLP

Shaoshi Dai [a,*], Bassam A. Younis [b], Liping Sun [a]

[a] Deep Water Engineering Research Center, Harbin Engineering University, 150001, China
[b] Department of Civil and Environmental Engineering, University of California, Davis, CA 95616 USA

ARTICLE INFO

Article history:
Received 15 February 2014
Accepted 14 April 2015
Available online 28 May 2015

Keywords:
OpenFOAM
Full-scale TLP
Vortex shedding
Hydrodynamics loads
Turbulence closure

ABSTRACT

OpenFOAM is an open-source finite-volume solver in the public domain. In recent years, its use for fluid-flow simulations has grown very rapidly due to its flexibility and extensive capabilities. However, to date, its application in ocean engineering has been very limited. The main purpose of this paper is to evaluate this tool for use in this field. Simulations were hence performed of the flow field around a full-scale Tension-Leg Platform (TLP) in steady current at high Reynolds number. Of particular interest was assessment of OpenFOAM's ability to accurately predict the unsteady hydrodynamic loads due to vortex shedding. Turbulence was accounted for using the $k-\varepsilon$ model. It was found that this model, which remains the model of choice in engineering practice, fails badly in this respect. A modification that has been shown to improve this model's performance in flows with vortex shedding was then implemented into OpenFOAM and checked against two benchmark flows namely around a single cylinder and around two cylinders in tandem. Application of the modified solver to the TLP flow convincingly demonstrates the suitability of this open-source tool, when used with the appropriate turbulence closure, for use in applications of interest to the ocean engineering community.

1. Introduction

The use of Computational Fluid Dynamics (CFD) as a tool for the design of floating structures is now widely accepted in the offshore industry and by the various certification agencies. This is due to the advances in computer technology that has made it possible to perform numerically well-resolved calculations on complex structures within reasonable turn-around times. It is also due to the availability of commercial CFD software that has leveraged advances in many fields (e.g. mesh generation, solution algorithms, and visualization) in packages that are convenient for use but whose source codes are inaccessible to the user. Apart from the uncertainty that arises from lack of knowledge of the inner workings of these packages, it is often difficult to adapt them to tackle a particular application, and nearly impossible to improve their performance via the incorporation of new findings. Moreover, the costs of licensing these packages appear to increase at the same rate as the decrease in the cost of the computer hardware used to run them. It is for these and other reasons that recent years have witnessed a rapid uptake by both the academic and the engineering design communities of OpenFOAM (www.openfoam.org) which is an open-source, finite-volume solver that is in the public domain. In keeping with the spirit of open access simulation tools, an enormous community of users of this software has emerged to rapidly exchange experiences and disseminate knowledge – a trend that is set to intensify with time. In contrast to the wide-spread use of OpenFOAM in other industries as well as in academic research, its adoption by the offshore engineering community has so far been somewhat limited. Notable exceptions are the studies by Chen et al. (2014), Lee et al. (2014), Lysenko et al. (2013) and Li et al. (2012), though some of these dealt mainly with idealized geometries. This lack of widespread use in industry is due, in part, to the absence of adequate demonstration of the utility of this tool for simulating the flows around the type of complex structures that are of practical relevance, at full scale and at high Reynolds number. This paper aims at making a contribution to the limited literature in this field with the intention of providing some bases for the assessment of the capabilities and limitations of OpenFOAM in offshore engineering. The benchmark flow adopted for this assessment is that which occurs around a full-scale Tension-Leg Platform (TLP). For reasons of cost and stability, this type of floating structure is widely used for deep-water operations such as in the Magnolia field in the Gulf of Mexico at a water depth of 1425 m, and in difficult areas such as the Norwegian Sea, and the South China Sea (Fang, 2010). A TLP consists of a floating structure formed by combination of circular columns and square-sectioned pontoons, tension cables and anchor leg system and relies on its own buoyancy to support the working load. These members are all prone to generating vortex shedding in their wakes. In most

* Corresponding author. Tel.: +86 0451 82569359.
E-mail address: daishaoshi@163.com (S. Dai).

http://dx.doi.org/10.1016/j.oceaneng.2015.04.042
0029-8018/

Nomenclature

B	Pontoon height
D	Column diameter
C_d	Drag coefficient $\left(=\frac{\overline{F_d}}{0.5\rho U_\infty^2 A}\right)$
C_{drms}	Fluctuating drag coefficient $\left(=\frac{\sqrt{\sum[F_d(t)-\overline{F_d}(t)]^2/N}}{0.5\rho {U_\infty}^2 A}\right)$
C_l	Lift coefficient $\left(=\frac{\overline{F_l}}{0.5\rho U_\infty^2 A}\right)$
C_{lrms}	Fluctuating lift force coefficient $\left(\frac{\sqrt{\sum[F_l(t)-\overline{F_l}(t)]^2/N}}{0.5\rho U_\infty^2 A}\right)$
F_d	In-line component of total force
F_l	Transvers component of total force
F_{lc}	Fluctuating lift force
f_s	Frequency of vortex shedding
H	Column height
H'	Draught
L	Characteristic length (D for circular section, w for square section)
p	Static pressure
P_k	Production of the turbulent kinetic energy
Q	Mean-flow kinetic energy $(=\frac{1}{2}U_iU_i)$
Re	Reynolds number$(=\frac{UD}{\nu})$
S	Distance between columns centers
St	Strouhal number $\left(=\frac{f_sD}{U_\infty}\right)$
t^*	Non-dimensional time $(=tU_0/D)$
U_∞	Velocity of incident flow
U_i	Mean velocity components
u_i	Fluctuating velocity components
u_τ	Friction velocity
$\overline{u_iu_j}$	Reynolds-stress tensor
W	Pontoon width

Greek

δ_{ij}	The Kronecker delta
Δt^*	Non-dimensional time-step $\left(=\frac{\Delta t * U_0}{D}\right)$
Δy	Normal distance from the wall
k	Turbulence kinetic energy
ε	Kinetic energy dissipation rate
κ	von Karman constant
μ	Dynamic viscosity
υ	Kinematic viscosity
υ_t	Eddy viscosity
ρ	Fluid density

Subscripts

i,j	Cartesian tensor indices
t	Turbulent

cases, the typical periods of the horizontal modes of motion (surge, sway and yaw) are of the order 1–2 min. This period is longer than the wave period, but the unsteady hydrodynamic loads induced are in this range and hence the risk of occurrence of structural resonance. Experimental data for isolated cylinders, both single and in tandem, are available in the subcritical regime (Zdravkovich, 1982; Yao and Chen, 1994; Bearman, 2011), but are scarce for the high Reynolds numbers found in practice and are almost totally absent for realistic TLP configurations. In this work, the strategy for assessment of OpenFOAM's capabilities and limitations for these configurations consists of quantitative demonstration of the numerical accuracy of the computations, comparisons with relevant experimental data, albeit for the simpler cases of isolated members, comparisons with results obtained by using a commercial CFD software, and examination of OpenFOAM's ability to capture the occurrence and consequences of vortex shedding. This strategy is pursued within the URANS framework wherein the solutions are obtained by solving suitably-averaged Navier–Stokes equations applicable to three-dimensional, unsteady flows. A turbulence closure is required to account for the effects of averaging and the precise closure adopted in this study is the $k-\varepsilon$ model which, due to its robustness and computational efficiency, remains the most widely used model in engineering design.

2. Mathematical formulations and computational method

The Open Source Field Operation and Manipulation (OpenFOAM) is a software library, written in C++, used to create applications such as the one created for the purpose of this research. An application consists of two categories: a *solver* which is designed to solve, by means of finite-volume methodology, the differential equations that describe a specific problem, and *utilities* where ancillary operations are performed (OpenFOAM Programmer's guide, 2012). In this work, the *solver* used was developed to solve the discretized forms of the equations that govern the conservation of mass and momentum in three dimensions. For incompressible flows, these equations are written using Cartesian tensor notation as:

Continuity:

$$\frac{\partial U_i}{\partial x_i}=0 \tag{1}$$

Momentum:

$$\frac{\partial U_i}{\partial t}+U_j\frac{\partial U_i}{\partial x_j}=\frac{\partial}{\partial x_j}(\nu\frac{\partial U_i}{\partial x_j}-\overline{u_iu_j})-\frac{1}{\rho}\frac{\partial p}{\partial x_i} \tag{2}$$

where U_i is the mean-velocity vector, u_i is the fluctuating velocity, p is the pressure, ν and ρ are, respectively, the kinematic viscosity and density. The turbulence correlations $\overline{u_iu_j}$ that appear in Eq. (2) are the unknown Reynolds stresses that are approximated by the turbulence closure described next.

The turbulence closure used in this study is of the eddy-viscosity type and is based on Boussinesq's assumption of linear stress–strain relationship to determine the unknown Reynolds stresses:

$$-\overline{u_iu_j}=\upsilon_t\left(\frac{\partial U_i}{\partial x_j}+\frac{\partial U_j}{\partial x_i}\right)-\frac{2}{3}\delta_{ij}k \tag{3}$$

where υ_t is the eddy viscosity which, in this study, is determined by reference to the turbulent kinetic energy (k) and its rate of dissipation by viscous action (ε):

$$\upsilon_t=C_\mu\frac{k^2}{\varepsilon} \tag{4}$$

where C_μ is a coefficient determined by reference to experimental data, and k and ε are obtained from the solution of their own transport equations which are given by:

$$\frac{\partial k}{\partial t}+U_j\frac{\partial k}{\partial x_j}=\frac{\partial}{\partial x_j}\left[\left(\upsilon+\frac{\upsilon_t}{\sigma_k}\right)\frac{\partial k}{\partial x_j}\right]+P_k-\varepsilon \tag{5}$$

$$\frac{\partial \varepsilon}{\partial t}+U_j\frac{\partial \varepsilon}{\partial x_j}=\frac{\partial}{\partial x_j}\left[\left(\upsilon+\frac{\upsilon_t}{\sigma_\varepsilon}\right)\frac{\partial \varepsilon}{\partial x_j}\right]+C_{\varepsilon1}\frac{\varepsilon}{k}P_k-C_{\varepsilon2}\frac{\varepsilon^2}{k} \tag{6}$$

where p_k is the rate of production of the turbulent kinetic energy:

$$p_k = \upsilon_t \frac{\partial U_i}{\partial x_j}\left(\frac{\partial U_i}{\partial x_j}+\frac{\partial U_j}{\partial x_i}\right) \tag{7}$$

In the above, $C_{\varepsilon 1}$, $C_{\varepsilon 2}$, σ_k, σ_ε are model coefficients whose values are listed in Table 1.

The $k-\varepsilon$ model as described above remains the most widely-used model in engineering practice but its utility for use in offshore engineering has not been adequately demonstrated. This model was developed by reference to data from statistically-stationary flows and thus the various coefficients that appear in its formulation ware calibrated using data from steady, attached, wall-bounded and free shear flows in approximate local equilibrium (Speziale, 1991). For the case of a TLP, the flow is unsteady and is characterized by the presence of large regions of reversed flow. It is also far from being in local equilibrium due to the presence of rapid and significant changes in the predominant direction of flow. It is therefore not surprising that it was found in several previous studies that this model fails badly in prediction of flows which, like the present, are dominated by vortex shedding (Murakami, 1993; Tsuchiya et al., 1997; Younis and Przulj, 2006). Specifically, the model fails in capturing the correct strength of vortex shedding as characterized, for example, by the root-mean-square values of the lift and drag coefficients of its various members. It was argued that this failure is a result of the model's inability to properly account for the effects of the interactions that occur between the periodic, large-scale fluctuations in the mean flow associated with the precession of the shed vortices, with the small-scale, random fluctuations that characterize the turbulent motions. Younis and Zhou (2006), from analysis of the process of spectral energy transfer in the presence of direct energy input at a discrete frequency, demonstrated that the model can be sensitized to the effects of this interaction by introducing a term into the ε equation that takes into the account the presence of a peak in the turbulence energy spectrum that represents the direct input of energy at the Strouhal frequency. Introduction of this new term in OpenFOAM proved to be a relatively straightforward task due to the accessibility of the source code. It was achieved simply by redefining the model coefficient $C_{\varepsilon 1}$ as follows:

$$C^*_{\varepsilon 1} = C_{\varepsilon 1}\left(1+C_t\frac{k}{\varepsilon}\frac{1}{Q+k}\left|\frac{\partial(Q+k)}{\partial t}\right|\right) \tag{8}$$

where Q is the mean-flow kinetic energy per unit mass and C_t is a coefficient whose value was determined in the original reference by numerical optimization (see Table 1). The modified model has already been shown to yield distinct improvements in the prediction of the closely-related flow around a three-dimensional surface-mounted square cylinder (Younis and Abrishamchi, 2014) but this study represents its first application to the flow around a TLP. In all cases, it was noted that that the increase in the computational time associated with the use of this modification was negligible.

Table 1
Turbulence model coefficients.

Turbulence model	C_μ	σ_k	σ_ε	$C_{\varepsilon 1}$	$C_{\varepsilon 2}$	C_t
Standard $k-\varepsilon$	0.09	1.00	1.30	1.45	1.90	–
Modified $k-\varepsilon$	0.09	1.00	1.30	1.45	1.90	0.38

In order to assess the utility of OpenFOAM for TLP applications in relation to alternative approaches, supplementary computations were obtained using CFX – a commercial software in wide use in the offshore industry. As with all commercial software, CFX is released only in executable form and hence it was not viable to introduce the modification to the ε equation with sufficient certainty. The two approaches were otherwise quite similar in that in both, the governing equations were discretized using finite-volume methodology, and solved iteratively using the PISO algorithm that couples the solution of the continuity and momentum equations to ensure that the predicted flow field satisfies both simultaneously. Second-order accurate schemes were used for discretization of both temporal and spatial gradients. Specifically, the convection terms were discretized with the Gauss integral discrete lattice, the Laplacian term was discretized using the Gauss linear corrected scheme, while the time discretization was by the implicit second-order accurate backward lattice scheme. Details of these schemes are given in the relevant users manuals.

3. Results and discussion

The modified turbulence model and its implementation into OpenFOAM were first checked for the benchmark case of the subcritical flow past a single circular cylinder. The solution domain is shown in Fig. 1 which also shows the non-uniformly distributed computational grid used for the simulations. The total computational elements were 94,935. All dimensions are referenced to the cylinder diameter. The boundary conditions employed for these simulations were as follows: at inlet, a uniform velocity was prescribed to give a Reynolds number $Re = 1.79 \times 10^5$. The value of relative turbulence intensity at inlet was set equal to 5%, which, with the assumption of isotropic turbulence, yields a value of turbulence kinetic energy $k_0 = 0.00375\ m^2/s^2$. The dissipation rate was obtained from the definition of eddy viscosity and by setting the ratio $(\nu_t/\nu) = 10$. The convergence criterion for the iterative process was set to be when absolute sum of all residuals fell to a value below 10^{-6}.

A snapshot of the predicted contours of the instantaneous pressure field around the cylinder, taken at the point of minimum lift, is shown in Fig. 2(a). These show the presence of a distinct vortex shedding process in the wake of cylinder. Fig. 2(b) shows the predicted velocity field at the same instant of time. Fig. 3 presents the time histories of lift and drag coefficients. These

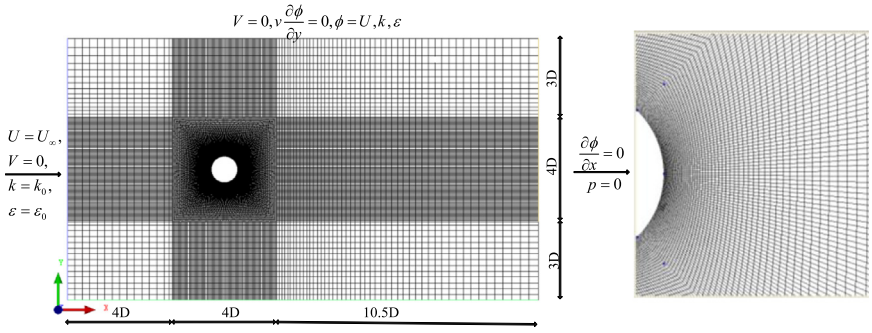

Fig. 1. Grid distribution of 2D cylinder for $Re = 1.79 \times 10^5$.

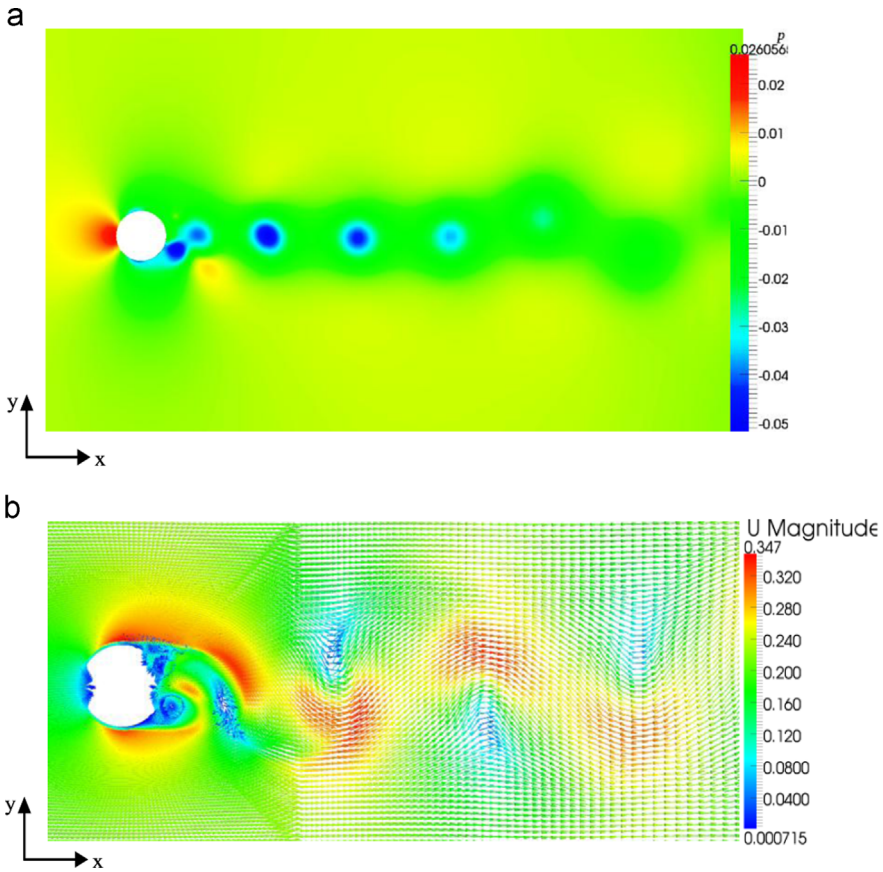

Fig. 2. Contours of pressure and velocity for 2D single cylinder (OpenFOAM) (a) Pressure field and (b) Velocity field.

parameters were defined with reference to the inlet velocity and the projected area of the cylinder. Table 2 shows the comparison between the predicted and measured non-dimensional parameters using both the standard and modified $k-\varepsilon$ models. It is evident from this table that the modified model yields results that are in close agreement with the experimental data. Computations obtained with CFX failed to capture the occurrence of vortex shedding altogether.

Further evaluation of the modified model is provided via simulation of the flow past two cylinders in tandem. This arrangement was studies experimentally by Gu and Sun (1999) and Okajima (1979). The case chosen here is for $S/D=1.7$ (S is the center-to-center distance between two cylinders) and $Re=2.2\times10^5$. The inlet turbulence intensity was set equal to 0.2% in accord with the experiments. The computational domain and the boundary conditions are shown in Fig. 4. The predicted contours of pressure and velocity around the two cylinders are shown in Fig. 5 and these reveal the presence of well-organized vortex-shedding field. Fig. 6 shows the predicted time history of the lift and drag coefficients for both cylinders. Due to the proximity of the two cylinders to each other, the intensity of oscillation of forces on the upstream cylinder is reduced relative to that on the downstream cylinder. Moreover, the drag coefficient for the aft cylinder is lower due to the shielding effect. Comparison between predicted and measured values is presented in Table 3 where it can be seen that the two are in close accord.

Attention is turned now to the computation of the full-scale TLP. Fig. 7 shows the extent of the computational domain. All dimensions are given relative to the column diameter (D). Due to the flow symmetry, only one half of the TLP is included. This simplification improves the quality of computational cells and hence the accuracy of simulations. The inlet to the computation domain was placed at a distance of 6D, and the exit was located at distance of approximate 40.5D from the down column center line. The TLP dimensions in the present simulation are listed in Table 4.

The computations were performed on a non-uniform structured meshes with three different grid densities. The smallest cell dimension in the x-y plane occurred near the TLP surfaces and was set equal to 0.01D. In the vertical direction (z), the smallest cell size on surface of column was 0.06D. The meshes were generated using the ICEM mesh generation package which is interfaced to OpenFOAM. They consisted of 494,525, 1,347,670 and 2,252,731 grid nodes – the numbers being selected to facilitate a quantitative assessment of the numerical errors in the simulations, as discussed below. Details of the mesh sizes are given in Table 5. Fig. 8 shows the surface nodes distribution as obtained with the finest mesh.

The boundary conditions of the computational domain were as follows. At inlet, the velocity of the incident current was assigned a constant value consistent with the required Reynolds number. The relative turbulence intensity level was also assumed to be uniform and was set equal to 0.05. The ratio of eddy to molecular viscosity was set equal to 100 and was used to determine the dissipation rate value at inlet. At the exit, fully-developed flow conditions were assumed so that the streamwise gradients of all dependent variables were set to zero. All remaining boundaries were treated as planes of symmetry. The surfaces of all members of the TLP were assumed to be smooth. The boundary conditions there were therefore obtained using the 'wall function' approach where it is assumed that the velocity close to the surface obeys the universal velocity distribution given by the standard logarithmic law of the wall:

$$\frac{U}{u_\tau}=\frac{1}{\kappa}\ln\left(E\frac{u_\tau\Delta y}{\upsilon}\right) \tag{9}$$

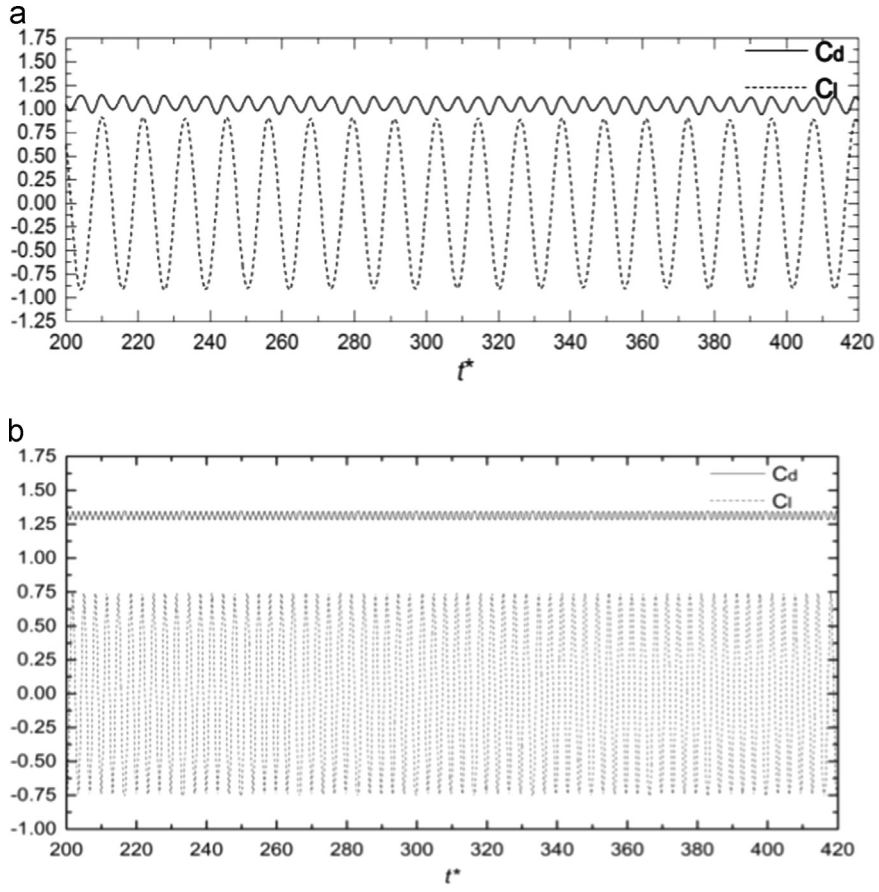

Fig. 3. Predictions of C_d and C_l with OpenFOAM and CFX (a) C_d and C_l as predicted with OpenFOAM (b) C_d and C_l as predicted with CFX.

Table 2
Predicted and measured bulk parameters of 2D single cylinder.

	St	$\overline{C}d$	$\overline{C}d_{rms}$	
Present work with modified $k-\varepsilon$ using OpenFOAM code	0.210	1.050	0.149	0.810
Present work with standard $k-\varepsilon$ using CFX code	0.30	1.315	0.025	0.500
Experimental results	0.184–0.192[a]	≈ 1.2[c]	–	0.800[e]
	≈ 0.2[b]	1.15-0.9[d]	–	0.870[f]

[a] Norberg (2003), $Re = 2.0 \times 10^5$.
[b] Roshko (1961) $Re < 3.5 \times 10^5$.
[c] DuarteRibeiro (1992), $Re = 0.4 \times 10^5$–3.5×10^5.
[d] Higuchi et al. (1989), $Re = 0.8 \times 10^5$–2.0×10^5.
[e] Drescher (1956), $Re = 1.0 \times 10^5$.
[f] Gerrard (1961), $Re = 1.8 \times 10^5$.

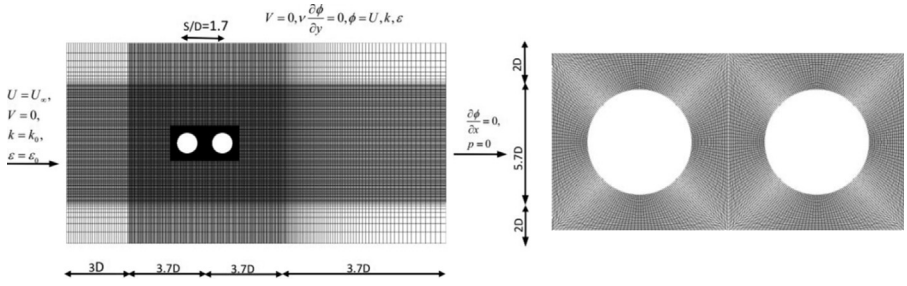

Fig. 4. Grid and boundary conditions for two cylinders in tandem.

where u_τ is the friction velocity and Δy is the normal distance from the wall to the centre of the grid nodes in contact with it. E and κ were assigned their usual values of 9.8 and 0.41, respectively. The non-dimensional time step for all the calculations Δt^* ($=\Delta t U_0/D$) was 0.0057.

Assessment of the numerical discretization errors is carried out using the Grid Convergence Index (GCI) method (Eca et al., 2007; Broadhead et al., 2004). The target parameters chosen for this purpose were the drag coefficient on the upstream and the downstream columns, and the Strouhal number. The analysis was

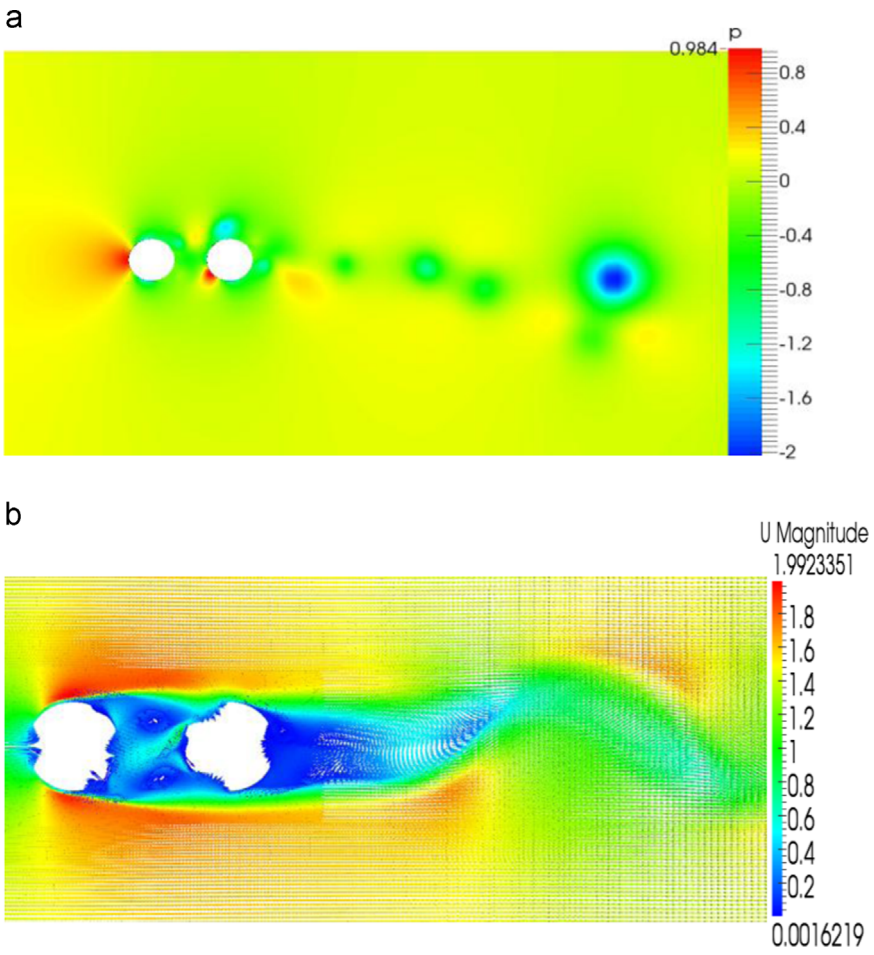

Fig. 5. Pressure and velocity distribution contour for 2D two cylinders in tandem using modified model (a) Pressure contour and (b) Velocity field.

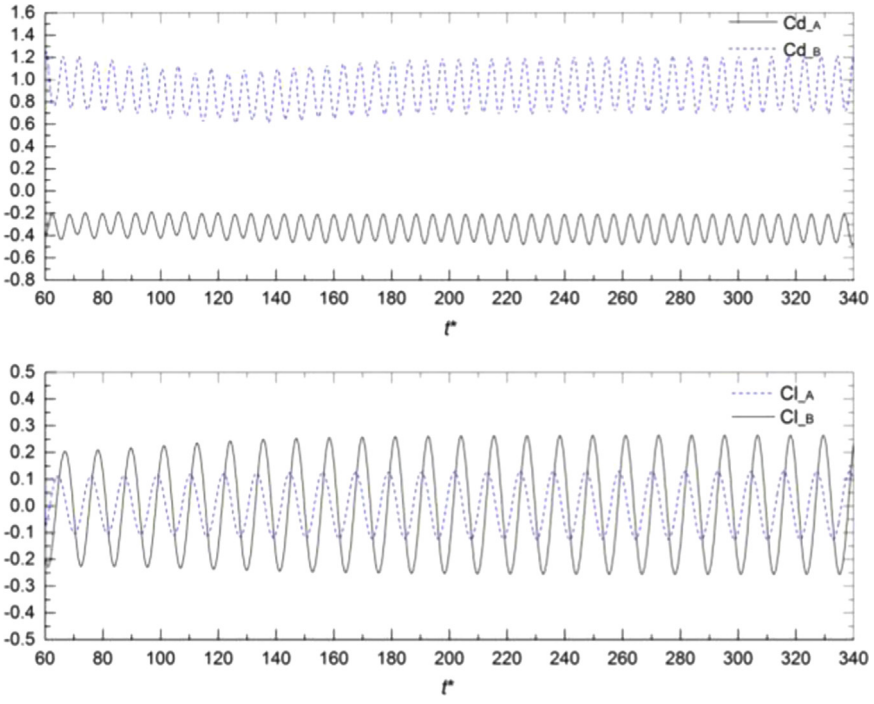

Fig. 6. Time histories of C_d and C_l of two cylinders in tandem ($S/d = 1.7$ and $Re = 2.2 \times 10^5$).

Table 3
Predicted and measured bulk parameters of two cylinders in tandem.

	St_A	St_B	$\overline{C}d_A$	$\overline{C}d_B$	$\overline{C}l_A$	$\overline{C}l_B$
Present work with modified $k-\varepsilon$ using OpenFOAM code	0.115	0.115	0.980	−0.321	0.004	0.003
Experimental results	–	–	0.97–1.0[a]	−0.35 to −0.4[a]	≈0[a]	≈0[a]
	≈0.120[b]	≈0.120[b]	1.04[b]	−0.17[b]	–	–

A reprensents front cylinder, and then B represents aft cylinder.
[a] Gu and Sun (1999), $Re = 2.2 \times 10^5$.
[b] Okajima (1979), $Re = 2.5 \times 10^5$.

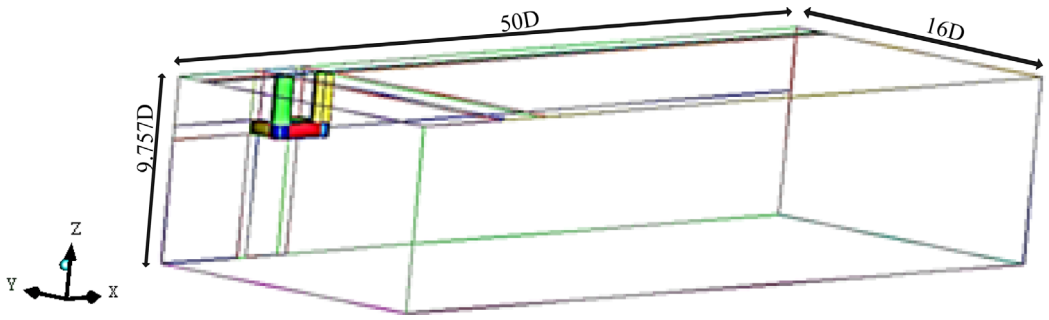

Fig. 7. Computational domain and block distribution.

Table 4
Dimensions of individual member of TLP.

Members	Parameter	Dimension (m)
Column height	H	22.25
Column diameter	D	8.75
Pontoon height	B	6.25
Pontoon width	W	6.25
Column separation distance	S	28.50
Draught	H'	28.50

Table 5
Grid details for TLP surface.

Grid size on cylinder surface	Nodes on cylinder	Total nodes
80 × 16	1280	494,525
160 × 16	2560	1,347,670
320 × 16	10,240	2,252,731

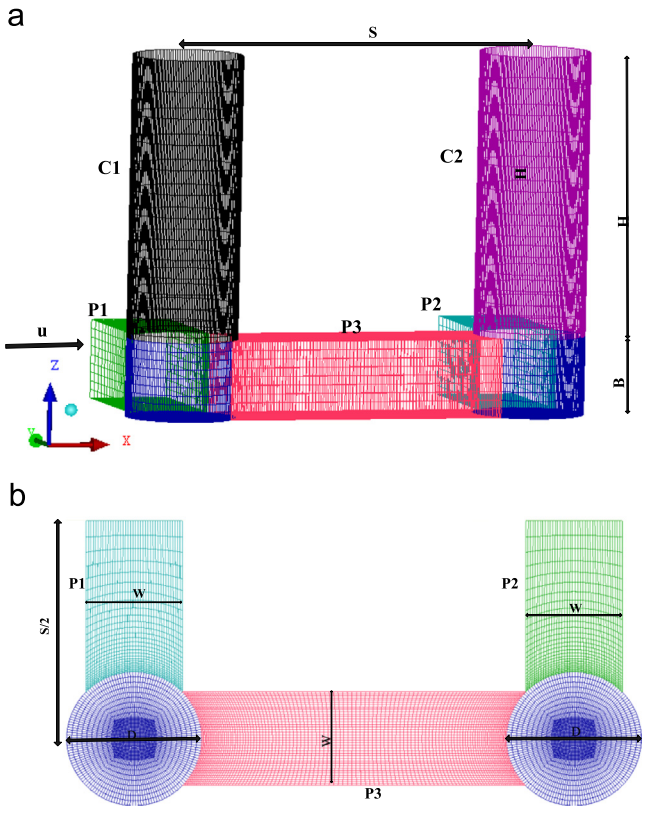

Fig. 8. Geometry model and grids distribution on surface of TLP.

performed for the case of Re of 7.5×10^6. The total non-dimensional simulation time (t^*) was 220 – a value which is sufficiently large for a periodic vortex-shedding process to be fully established. This method has now become widely accepted as a reliable means to estimate the discretization errors in computational fluid dynamics. It is based on the well-known Richardson Extrapolation method, which mainly calculates the extrapolated values (ϕ_{ext}^{21}) and fine-grid convergence index (GCI_{fine}^{21}) according to global cell size or local cell size. The detailed procedure can be found in Celik et al. (2008). Based on the outcome of applying the GCI method, the discretization error for value of Cd was less than 10% (see Table 6).

Consideration is turned now to the predicted flow field around the TLP. The principal features of the flow are the occurrence of vortex shedding from all members, and the large modification to the flow field that arises when shedding from upstream members interact with those from downstream. The predicted velocity vectors at horizontal cross section of column length are shown in Fig. 9(a) and b). It can be seen from Fig. 9(a) that the predicted flow field is strongly asymmetric due to the influence of the adjacent pontoons. Further downstream, the asymmetry becomes less noticeable.

Fig. 10 shows the computed time histories of the lift and drag coefficients for both the front and aft columns. Results are presented for both OpenFOAM and CFX, and for both the standard and modified models. The plots in Fig. 10(a1) and (b1) show significant differences between the results obtained with the two solvers. The oscillations of both C_d and C_l as predicted by CFX are very weak, especially for the front column. Moreover, from Fig. 10

(a2), (a1) and Fig. 10(b2), (b1), it is clear that OpenFOAM with the modified turbulence model produces a clearly periodic and well-organized shedding process. In the TLP geometry under consideration, where the distance between the two columns centers is $S/D=3.257$, what appears to be an intermittent vortex shedding field is produced whereby there exists two kinds of alternating signals from time history of C_l (Fig. 10) This bi-stable flow was captured only with the modified $k-\varepsilon$ model. When the separated flow from the upstream column interacts with the downstream one, a negative drag force is generated such that the drag coefficient is now significantly lower than for an isolated cylinder. Comparing C_l value between the front column and aft column (see Fig. 10), it is evident that the value of front column is finite while that for the aft column oscillates is only marginally different from zero. Due to the deflection effect of wake flow of the front column noted earlier, C_l value of which is negative (see Fig. 9 and Fig. 10 (a2)).

Table 7 presents the predicted time-averaged values of the drag and lift coefficients ($\overline{C_d}$ and $\overline{C_l}$) as obtained with both the standard and the modified turbulence models. The most noticeable result seen there is the reduction of $\overline{C_d}$ for the aft column, and the nonzero value of $\overline{C_l}$ for both columns. Younis et al. (2001) also found this reduction of $\overline{C_d}$ value when he studied character of global drag force (C_x) for TLP at different angles of incidence. The value of $\overline{C_d}$ for the front column obtained in that study is somewhat greater than that obtained here with the modified $k-\varepsilon$, but the results for the aft column are quite similar. Yao et al. (1994) measured the drag force of tandem cylinders in a uniform current and reported a value of $\overline{C_d}$ for the front cylinder of 0.42. Under the same Reynolds number ($5.2\times5.8\times10^5$), global drag force (C_x) reported by Younis et al. (2001) was 0.51. It is noted that the influence of the angle of incidence is to increase the drag. This difference is well explained the differences between predicted reductions in present paper with others. In addition, the guidelines from the DNV design (DNV Classification Note, 1993) manual give the drag coefficient for columns as 0.56 after allowing for the effects of incidence. In contrast, the $\overline{C_d}$ value calculated by modified $k-\varepsilon$ much closer to DNV values. For aft column, the $\overline{C_d}$ value is smaller than the value of front column, but it is very approximate with experimental value by Zdravkovich and Pridden (1977) for two cylinders ($L/D=3.25$), which is about 0.385. Regarding the time-averaged lift coefficient ($\overline{C_l}$), It is clear that the different turbulence models yield approximately similar values.

Table 8 compares the predicted root-mean-square values of the drag and lift coefficients (C_{drms} and C_{lrms}). Due to interaction with the vortex shedding that occurs from the front column, the fluctuating forces for the aft column are larger than those for the front column. The standard $k-\varepsilon$ model predicts almost zero fluctuations on the front column in sharp contrast with the modified model which predicts a significantly high value for C_{lrms}.

An important parameter in TLP design is the frequency at which the vortex-shedding occurs. This was obtained here by performing Fast-Fourier Transform on the time series of the fluctuating lift coefficients to obtain the power spectrum for both the front and aft columns (C_1, C_2 in Fig. 8). Fig. 11(a) shows these time series for $\mathrm{Re}=7.5\times10^7$. Due to the interaction with the vortices that are shed from the front column, the fluctuating lift force on the aft column is significantly greater as can be seen from Fig. 11(b). The spectra also show the presence of three frequencies peaks. The highest peak corresponds to the dominant frequency which gives a Strouhal number $St=0.157$. The local peak which

Table 6
The GCI method estimates of discretization errors.

Variables/Parameters	$\phi=C_{d1}$ (C1)	$\phi=C_{d2}$ (C2)	$\phi=St$
$N_1,\ N_2,\ N_3$	2,252,731, 1,347,670, 494,525		
r_{21}	1.18679	1.1868	1.1868
r_{32}	1.39704	1.3971	1.3971
ϕ_1	0.40800	0.336	0.250
ϕ_2	0.41700	0.356	0.241
ϕ_3	0.47700	0.383	0.161
p	4.57940	5.0691	5.220
ϕ_{ext}^{21}	0.40040	0.3215	0.258
e_{ea}^{21}	0.02206	0.0595	0.040
e_{ext}^{21}	0.01887	0.045	0.027
GCI_{fine}^{21}	0.02316	0.054	0.034

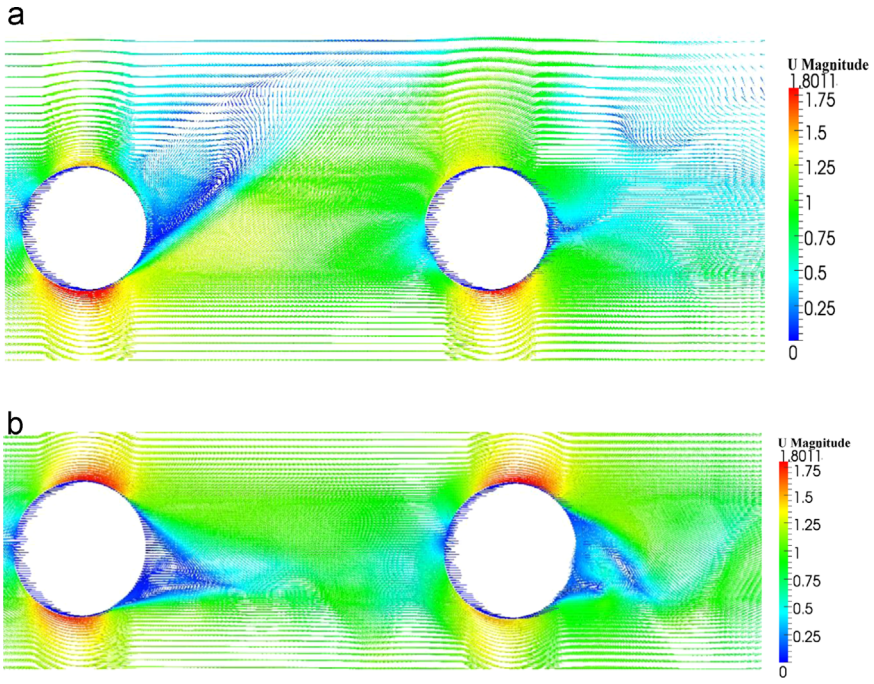

Fig. 9. Predicted velocity distributions at different heights along column with modified $k-\varepsilon$ model ($Re=7.5\times10^6$) (a) $Z=8.125D$ and (b) $Z=8.94D$.

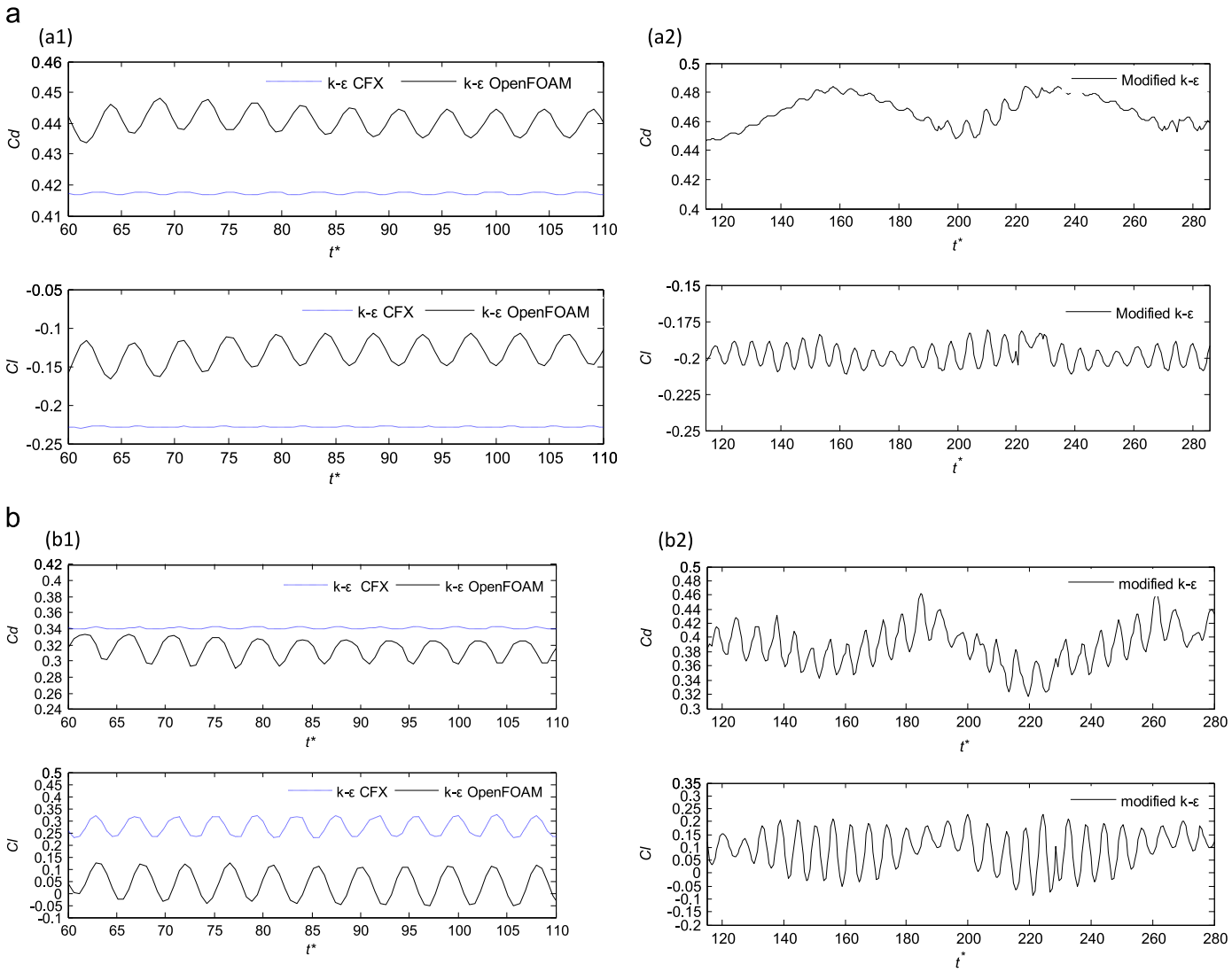

Fig. 10. Predicted time histories of C_d and C_l on columns using standard $k-\varepsilon$ (a1, b1) and modified $k-\varepsilon$ model (a2, b2) ($Re = 7.5 \times 10^6$) (a) Front column and (b) Aft column.

Table 7
Comparison of $\overline{C_d}$ and $\overline{C_l}$ from different codes ($Re = 7.5 \times 10^6$).

Turbulence model	$\overline{C_d}$		$\overline{C_l}$	
	Front column (C1)	Aft column (C2)	Front column (C1)	Aft column (C2)
$k-\varepsilon$ (CFX)	0.417	0.342	−0.232	0.275
$k-\varepsilon$ (openFOAM)	0.439	0.320	−0.204	0.04
Mod $k-\varepsilon$ (openFOAM)	0.470	0.399	−0.200	0.09
Younis et al. (2001, $Re = 2 \times 10^7$)	0.790	0.490	–	–
Yao et al. (1994, $Re = 5.8 \times 10^5$)	0.420	0.165	0	0
DNV (average values)	0.56		–	

Table 8
Comparison of C_{drms} and C_{lrms} on columns from different codes and turbulence models.

Turbulence model	C_{drms}		C_{lrms}	
	Front column (C1)	Aft column (C2)	Front column (C1)	Aft column (C2)
$k-\varepsilon$ (CFX)	0.001	0.005	0.003	0.004
$k-\varepsilon$ (openFOAM)	0.004	0.020	0.0036	0.015
Mod $k-\varepsilon$ (openFOAM)	0.011	0.030	0.007	0.073

appears at $St = 0.012$ represents the attachment frequency of shear layer separation from the front column. The other local maximum at $St = 0.18$ represents secondary vortices in its spectrum. These results suggest that the dominant frequency of the forces that act upon the TLP is much lower than that of a single cylinder which is at St of 0.22–0.29 for Re of $Re = (4-7.1) \times 10^6$ (Schewe, 1983; James et al., 1979). Fig. 12 shows the spectrum of both columns as obtained by using the standard $k-\varepsilon$ model. The dominant frequency is at St of 0.22–0.25 unlike the spectrum of the modified $k-\varepsilon$ model, so this turbulence model failed to predict the reliable frequency of vortex shedding. In contrast to the distinct vertex shedding that occurs from both columns, no vortex shedding was observed to occur from either the front or aft pontoons (P1 and P2 in Fig. 8).

Fig. 13 presents the velocity distribution at a horizontal cross section in the middle of pontoon's height. Reversed flow appears in the corner between the front pontoon (P1) and the horizontal

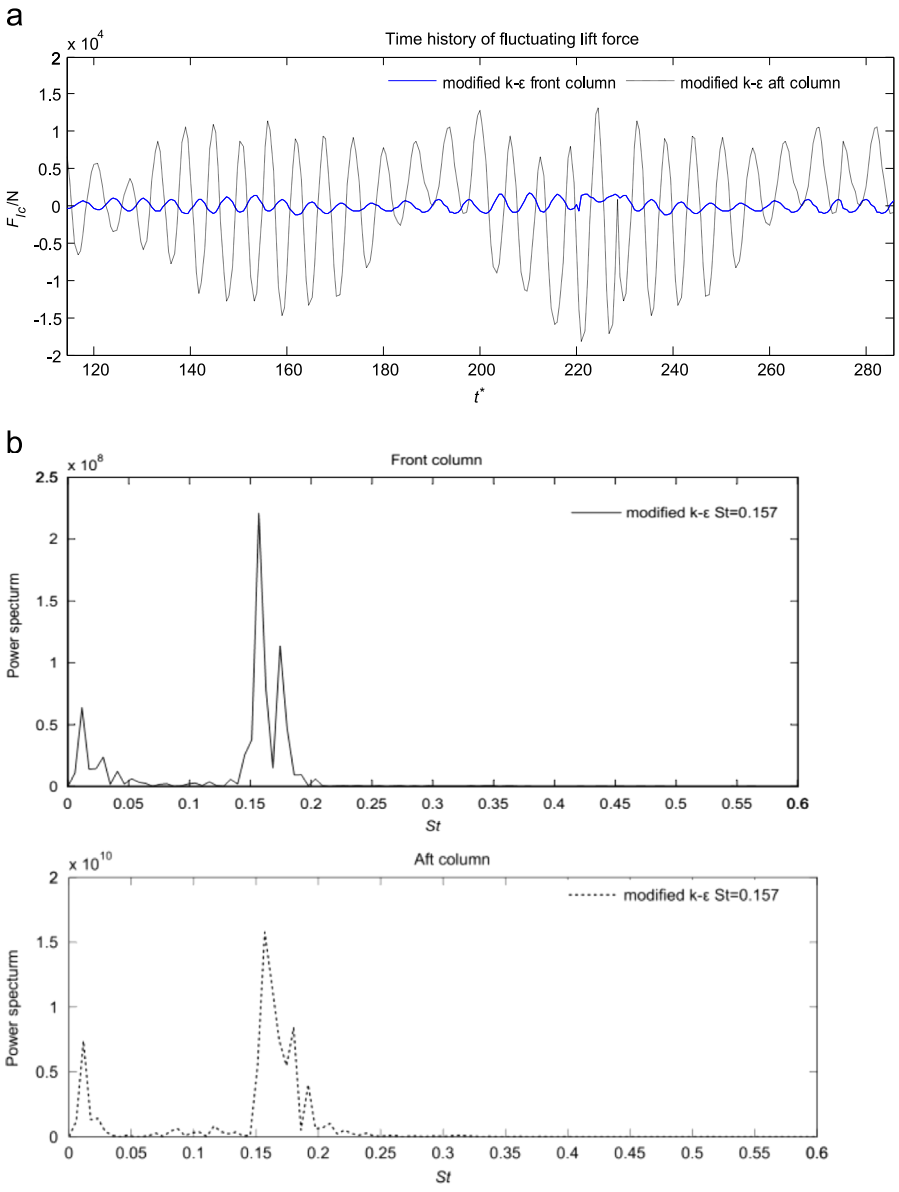

Fig. 11. Predicted power spectrums of fluctuating lift forces with the modified $k-\varepsilon$ model.

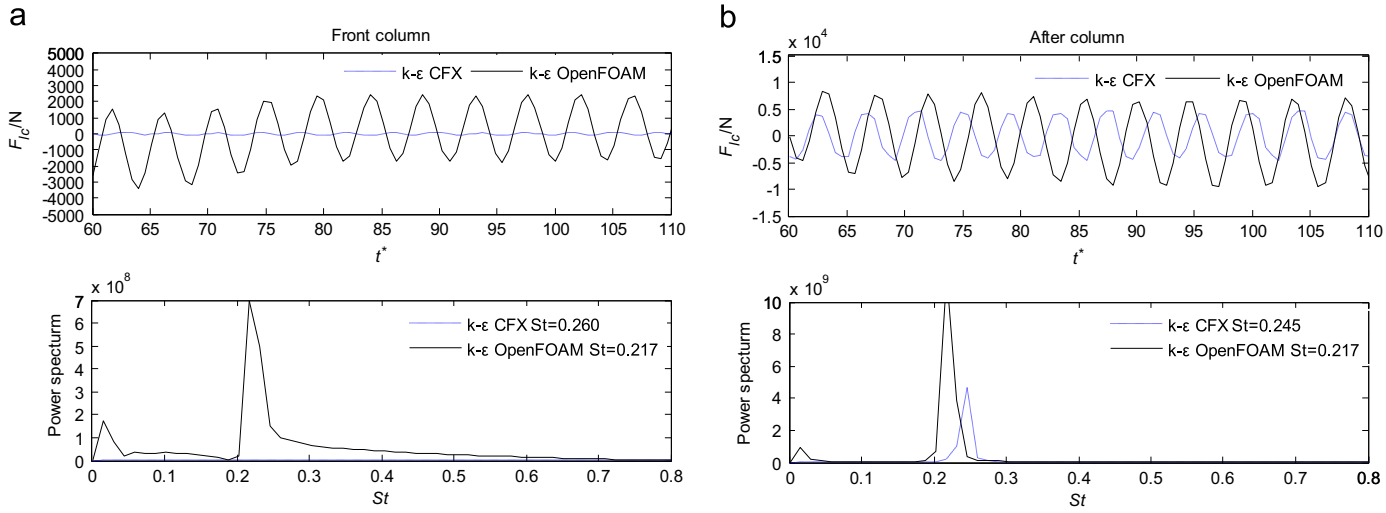

Fig. 12. Predicted power spectrums of fluctuating lift forces for both columns using the standard $k-\varepsilon$ model.

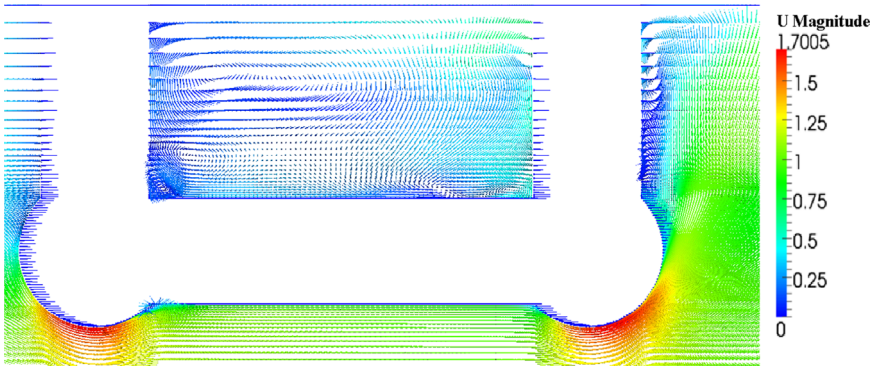

Fig. 13. Velocity vector distributions at mid-height of pontoons.

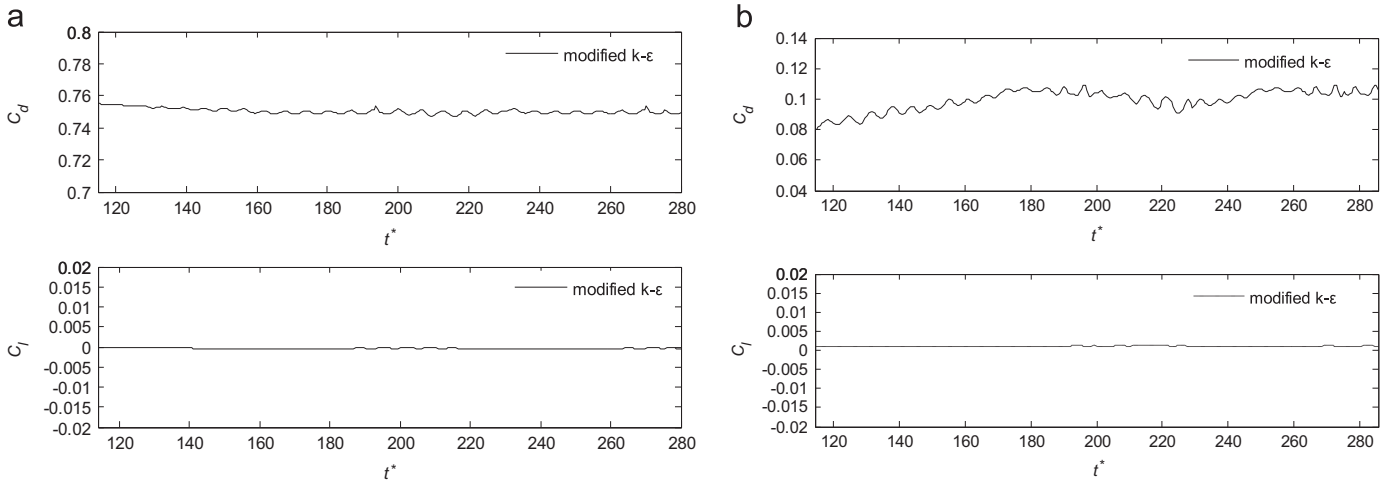

Fig. 14. Predicted time histories of C_d and C_l on pontoons with modified $k-\varepsilon$ model (a) Upstream pontoon (P1) and (b) Downstream pontoon (P2).

Table 9
Comparison of $\overline{C_d}$ and $\overline{C_l}$ on columns using different solvers and turbulence models.

Turbulence model	$\overline{C_d}$			$\overline{C_l}$		
	P1	P2	P3	P1	P2	P3
$k-\varepsilon$ (CFX)	0.640	0.135	0	0	0	0.702
$k-\varepsilon$ (openFOAM)	0.710	0.08	0	0	0	1.180
Mod $k-\varepsilon$ (openFOAM)	**0.720**	0.09	0	0	0	1.170
RNG (Younis et al., 2001)	0.790	0.18	0	0	–	–
Experiments (Sakamoto and Haniu, 1988)	1.025	0.06	–	–	–	–

pontoon (P3), as would be expected due to the high pressure gradients that occur there.

Fig. 14 shows the predicted time histories of C_d and C_l on the pontoons obtained by using modified $k-\varepsilon$ turbulence model. It is clear that the fluctuating drag forces on both pontoons are very weak. Due to the larger velocity difference on either side of the upstream pontoon, its drag coefficient is quite large. The lift force coefficients of both pontoons are zero because of obstructed effect of horizontal pontoon (P3).

Comparison of the predicted $\overline{C_d}$ values for the pontoons obtained with the two flow solvers is shown in Table 9. The predicted $\overline{C_d}$ value for the upstream pontoon was about 0.72 for *Re* of 7.5×10^6, which is nearly twice the value for the front column. Younis et al. (2001) reported the global drag force coefficient for the same TLP. Their results, which are presented in Table 9, are broadly similar to the present ones.

4. Conclusions

An assessment of the suitability of OpenFOAM, an open-source simulations tool that is in the public domain, for use in offshore design applications has been carried out. The benchmark problem chosen for this assessment was that of the flow around a full-scale TLP at high Reynolds number. The numerical accuracy of the results was assessed using the Grid Convergence Index method. The results were compared with previously published experimental data, and with computer simulations for both single isolated cylinders and for the full-scale TLP. Supplementary computations were performed using a commercial solver of the type in common use in the offshore industry. It was found necessary to modify the standard $k-\varepsilon$ model in order to correctly capture the occurrence and strength of vortex shedding from the various members. The modification accounts for the effects of the interactions between the periodic vortex shedding and the random fluctuations that characterize the turbulent motions. Implementation of this modification into OpenFOAM proved to be fairly straightforward due to the open-source nature of the software. This is in contrast to the commercial simulations software which is supplied only in executable form and which therefore failed entirely in capturing this

defining feature of the flow. The results of this study confirm that that an open-source flow solver that is in the public domain can be used with confidence in the design of full-scale TLPs provided that the turbulence model used is capable of account for the effects of vortex shedding on the turbulent motions.

Acknowledgments

We gratefully acknowledge the support provided by the National Natural Science Foundation of China (Grant no. 11472087 and No. 11002038), the National Science foundation of Heilongjiang Province (Grant no. E201207).

References

Bearman, P.W., 2011. Circular cylinder wakes and vortex-induced vibrations. J. Fluids Struct. 27, 648–658.
Broadhead, B.L., Rearden, B.T., Hopper, C.M., Wagschal, J.J., Parks, C.V., 2004. Sensitivity and university-based criticality safety validation techniques. Nucl. Sci. Eng. 146, 340–366.
Celik, I.B., Ghia, U., Roache, P.J., Freitas, C.J., Coleman, Hugh, Read, P.E., 2008. Procedure for estimation and reporting of uncertainty due to discretization in CFD applications. J. Fluids Eng. 130, 078001-1–078001-4.
Chen, L.F., Zang, J., Hillis, A.J., Morgan, G.C.J., Plummer, A.R., 2014. Numerical investigation of wave-structure interaction using OpenFOAM. Ocean Eng. 88, 91–109.
DNV Classification Note, 1993, Environmental conditions and environmental loads, No. 30.5.
Drescher, H., 1956. Messung der auf querangestromte zylinder ausgeubten zeitlich veranderten drucke. Z. Fluggwissenschaften 4, 17–21.
DuarteRibeiro, J., 1992. Fluctuating lift and its spanwise correlation on a circular cylinder in a smooth and in a turbulent flow: a critical review. J. Wind Eng. Ind. Aerodyn. 40, 179–198.
Eca, L., Hoekstra, M., Roache, P.J., 2007. Verification of calculations an overview of the 2nd Lisbon workshop on CFD uncertainty analysis. In: Proceedings of the AIAA Computational Fluid Dynamics Conference. Miami, FL, June 2007, AIAA Paper No. 2007-4089.
Fang, H.C., 2010. A new development of deep-water platform for petroleum equipment. China Ocean Platf. 25, 1–7.
Gerrard, J.H., 1961. An experimental investigation of the oscillating lift and drag of a circular cylinder shedding turbulent vortices. J. Fluid Mech. 11, 244–256.
Gu, Z.F., Sun, T.F., 1999. On interference between two circular cylinders in staggered arrangement at high subcritical Reynolds numbers. J. Wind Eng. Ind. Aerodyn. 80, 287–309.
Higuchi, H., Kim, H.J., Farell, C., 1989. On flow separation and reattachment around a circular cylinder at critical Reynolds numbers. J. Fluid Mech. 200, 149–171.
James, W.D., Paris, S.W., Malcolm, G.N., 1979. A study of viscous cross-flow effects on circular cylinders at high Reynolds numbers. AIAA J. 18, 1066–1072 79-1477.
Lee, A.H., Campbell, R.L., Hambric, S.A., 2014. Coupled delayed-detached-eddy simulation and structural vibration of a self-oscillating cylinder due to vortex-shedding. J. Fluids Struct. 48, 216–234.
Li, Y.L., Zhu, R.C., Miao, G.P., Fan, J., 2012. Simulation of tank sloshing based on OpenFOAM and coupling with ship motions in time domain. J. Hydrodyn. Ser. B 24, 450–457.
Lysenko, D.A., Ertesvag, I.S., Rian, K.E., 2013. Modeling of turbulent separated flows using OpenFOAM. Comput. Fluids 80, 408–422.
Murakami, S., 1993. Comparison of various turbulence models applied to a bluff body. J. Wind Eng. Ind. Aerodyn. 46–47, 21–36.
Norberg, C., 2003. Fluctuating lift on a circular cylinder: review and new measurements. J. Fluids Struct. 17, 57–96.
Okajima, A., 1979. Flows aroud two tandem circular cylinders at very high Reynolds numbers. Bull. JSME 22, 504–511.
OpenFOAM Programmer's guide, 2012. Version 2.2.1. 2012. 5, The OpenFOAM Foundation (http://www.openfoam.org).
Roshko, A., 1961. Experiments on the flow past a circular cylinder at very high Reynolds number. J. Fluid Mech. 10, 345–356.
Sakamoto, H., Haniu, H., 1988. Aerodynamic forces acting on two square prisms placed vertically in a turbulent boundary layer. J. Wind Eng. Ind. Aerodyn. 31, 41–66.
Schewe, G., 1983. On the force fluctuations acting on a circular cylinder in crossflow from subcritical up to transcritical Reynolds numbers. J. Fluid Mech. 133, 265–285.
Speziale, C.G., 1991. Analytical methods for the development of Reynolds-stress closures in turbulence. Annu. Rev. Fluid Mech. 23, 107–157.
Tsuchiya, M., Murakami, S., Mochida, A., Kondo, K., Ishida, Y., 1997. Development of a new k–ε model for flow and pressure fields around bluff body. J. Wind Eng. Ind. Aerodyn. 67–68, 169–182.
Yao, X.L., Chen, Q.F., 1994. Overview of vortex induced vibration for tandem cylinder in uniform flow. J. Harbin Shipbuild. Eng. Inst. 15, 1–16.
Yao, X.L., Chen, Q.F., Xu, W.J., 1994. Experimental study on the characteristics of vortex induced vibration of tandem cylinders in uniform flow. J. Vib. Eng. 7, 17–22.
Younis, B.A., Abrishamchi, A., 2014. Three-dimensional turbulent vortex shedding from a surface-mounted square cylinder: predictions with Large-Eddy Simulations and URANS. J. Fluids Eng. 136, 060907.
Younis, B.A., Przulj, V., 2006. Computation of turbulent vortex shedding. Comput. Mech. 37, 408–425.
Younis, B.A., Teigen, P., Przulj, V.P., 2001. Estimating the hydrodynamic forces on a mini design-code techniques. Ocean Eng. 28, 585–602.
Younis, B.A., Zhou, Y., 2006. Accounting for mean-flow periodicity in turbulence closures. Phys. Fluids 18, 018102–018105.
Zdravkovich, M.M., 1982. Smoke observation of wakes of tandem cylinders at low Reynolds number. Aeronaut. J. 76, 108–114.
Zdravkovich, M.M., Pridden, D.L., 1977. Interference between two circular cylinders; Series of unexpected discontinuities. J. Wind Eng. Ind. Aerodyn. 2, 255–270.